PERGAMON

Journal of Structural Geology 25 (2003) 867–881

JOURNAL OF STRUCTURAL GEOLOGY

www.elsevier.com/locate/jstrugeo

Role of décollement material with different rheological properties in the structure of the Aljibe thrust imbricate (Flysch Trough, Gibraltar Arc): an analogue modelling approach

María Luján[a,*], Fabrizio Storti[b], Juan-Carlos Balanyá[a], Ana Crespo-Blanc[a], Federico Rossetti[b]

[a]*Departamento de Geodinámica, Instituto Andaluz de Ciencias de la Tierra, Universidad de Granada—CSIC, 18071 Granada, Spain*
[b]*Dipartimento di Scienze Geologiche, Universitá "Roma Tre", Largo S. L. Murialdo 1, 00146 Rome, Italy*

Received 31 October 2001; received in revised form 24 June 2002; accepted 26 June 2002

Abstract

The Miocene Aljibe thrust imbricate (Flysch Trough), in the external zone of the Gibraltar Arc, shows large changes in structural style towards the foreland. Rheological variation of the décollement rocks—Triassic evaporitic rocks and Mesozoic limestones—appears to be the main factor controlling the contrasts in structural style that characterise adjacent wedge domains. In order to test this hypothesis, we carried out analogue experiments involving three-dimensional variations of décollement material. A plate of viscous material was placed in the central part of the models, at the base of the sand multilayers. Different geometries of the viscous plate were used. Experimental results show a strong link between the rheological properties of the décollement material and the structure of the overlying thrust wedge. These results compare well with the internal geometry and vergence distribution in the Aljibe thrust imbricate. Indeed, the tectonic style of the wedge can be explained as a consequence of variations of rock type along the basal décollement.

Keywords: Analogue modelling; Thrust imbricate; Décollement; Vergence distribution; Aljibe unit

1. Introduction

Variability in vergence and tectonic style both along and across the structural trend of fold-and-thrust belts can be related to the frictional or viscous behaviour of the main décollement levels, as shown in the Jura mountains (Laubscher, 1972), the Zagros (Colman-Saad, 1978), the Spanish Pyrenees (Burbank et al., 1992), the Parry Islands Foldbelt (Harrison and Bally, 1988), the Salt Range (Butler et al., 1987), or the Mediterranean Ridge (Ryan et al., 1982). Indeed, incompetent décollement rocks, like evaporites or shales, enhance the delocalisation and outward propagation of deformation (e.g. Geiser, 1988; Macedo and Marshak, 1999), and the growing fold-and-thrust belts attain extremely narrow surface tapers (Davis and Engelder, 1985). Thrust faults and folds within thrust wedges accreting above low-friction basal décollements generally have no preferred vergence (Davis and Engelder, 1985), and very complex geometries can develop (e.g. Velaj et al., 1999).

The Aljibe thrust imbricate, which is the main tectonic unit of the Flysch Complex, in the external zone of the Gibraltar Arc (Betic–Rif orogenic belt), provides an example of such structural complexity (Fig. 1). The pre-contractional, three-dimensional (3D) geometry of décollement materials with different rheological properties appears to be a key parameter controlling the structure and vergence partitioning in the developing foreland belt. To gain insights as to the role of this parameter, we performed sandbox analogue experiments. The efficiency of analogue modelling for studying the influence of incompetent décollement rocks under different boundary conditions on the evolution of fold-and-thrust belts has been widely proven (Cobbold et al., 1989, 1995; Dixon and Liu, 1992; Talbot, 1992; Letouzey et al., 1995; Bonini et al., 2000; Cotton and Koyi, 2000, among others). Our experiments contribute to broaden the available experimental templates for natural thrust wedges. The fact that structural variations obtained in the models compare with those observed in the study area throws a new light on the 3D distribution of décollement rocks at the base of the Aljibe thrust imbricate.

* Corresponding author. Tel.: +34-9-58-243158; fax: +34-9-58-243384.
E-mail address: mlujan@ugr.es (M. Luján).

0191-8141/03/$ - see front matter © 2002 Elsevier Science Ltd. All rights reserved.
PII: S0191-8141(02)00087-1

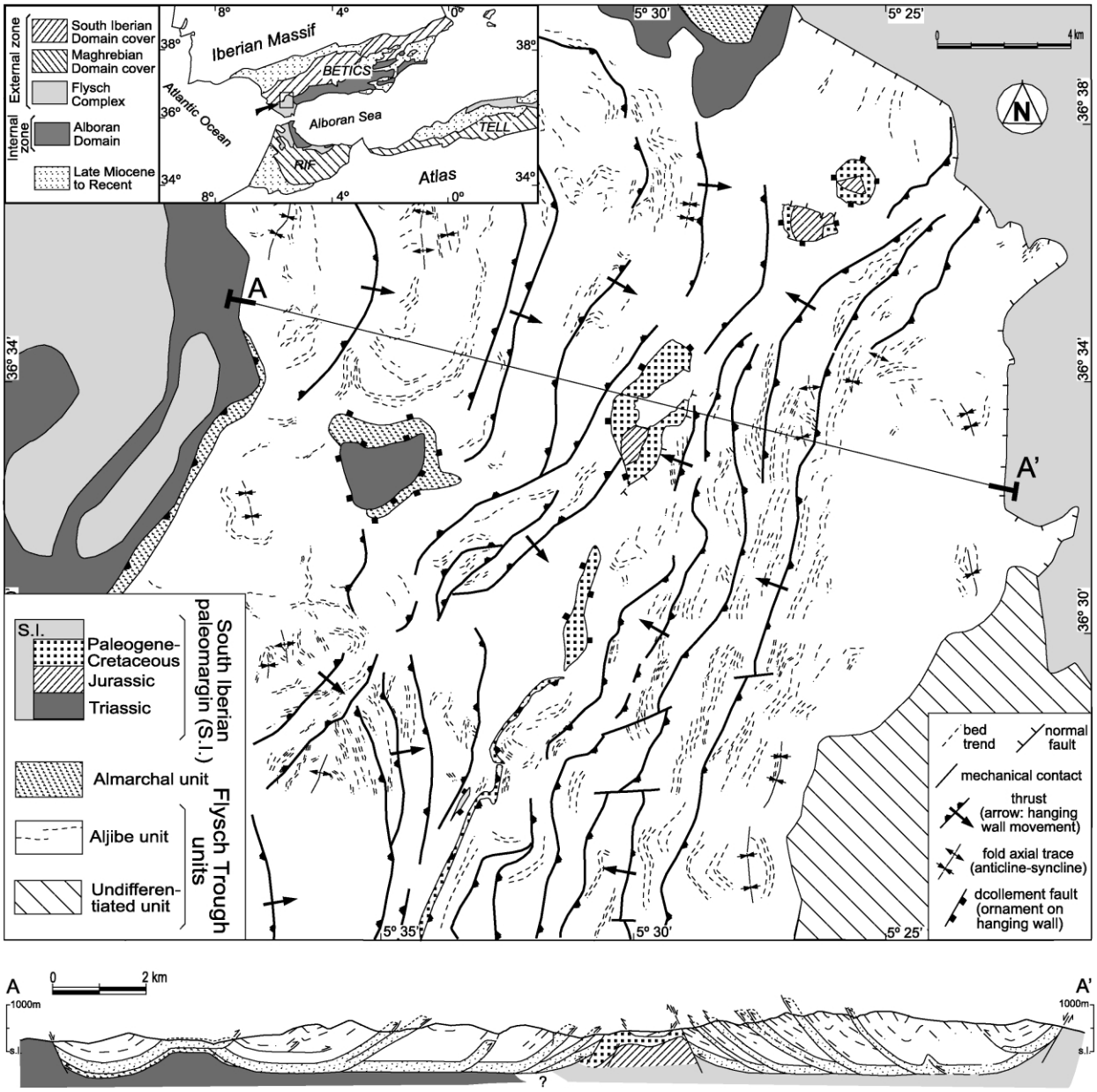

Fig. 1. Structural map of the Aljibe unit. Cross-section illustrating the various style of deformation. Inset: main tectonic complexes in the Gibraltar Arc (rectangle: study area).

2. The Gibraltar Arc and the structure of the Aljibe Unit

The external zones within the Gibraltar Arc formed as an arcuate fold-and-thrust belt due to the overall westward emplacement of continental metamorphic rocks belonging to the Alboran Domain (Betic–Rif hinterland) over the external domain: the South Iberian and Maghrebian paleomargins (inset of Fig. 1). The emplacement produced the obliteration of the Flysch Trough during the Miocene (Balanyá and García-Dueñas, 1988). This deep trough developed on a transform zone of attenuated continental lithosphere, eventually oceanic (Durand-Delga et al., 2000), situated between the African and European plates and filled by sediments from Cretaceous to Neogene times.

In the northern branch of the Gibraltar Arc (inset of Fig. 1), the units that belong to the Subbetic cover are derived from the South Iberian paleomargin, composed of Triassic to Cenozoic rocks. During the Early to Middle Miocene, these rocks were detached from their Hercynian basement and formed allochthonous units, shortened by WNW- to NW-vergent folds and thrusts (e.g. Bourgois, 1978; Crespo-Blanc and Campos, 2001, and references therein).

In the study area, the Subbetic sedimentary sequence comprises: (a) a Triassic sequence of limestones and dolomitised carbonate rocks (Muschelkalk facies), together with gypsiferous claystones and fine-grained sandstones (Keuper facies); (b) a Jurassic sequence of dolomite rocks and overlying massive, predominantly shallow marine

Table 1
Nature and model parameters. The data are taken from the papers listed below the table

Parameter	Nature (N)	Model (M)	Scaling factor (N/M)
Length l (m)	1×10^{3}	5×10^{-3}	2×10^{5}
Density ρ_v (kg m^{-3})	2300 (a)	1300	1.77
Density ρ_b (kg m^{-3})	2400 (b)	1500	1.60
Viscosity η (Pa s)	$1.7 \times 10^{18 \text{ to } (19)}$ (c)	1.2×10^{5}	$1.42 \times 10^{13 \text{ to } (14)}$
Gravity g (m s^{-2})	9.81	9.81	1
Stress σ (Pa)	$\rho_{b_N} \times g_N \times l_N$ (d)	$\rho_{b_M} \times g_M \times l_M$ (d)	3.2×10^{5}
	2.35×10^{7}	73.57	
Time t (s)	$t_N = \eta_N/\eta_M(\rho_M g_M l_M/\rho_N g_N l_N)t_M$ (d)	3600	$3.21 \times 10^{8 \text{ to } (9)}$
	$1.14 \times 10^{12 \text{ to } (13)}$ ($\sim$0.04–0.4 Ma)		
	$\nu_N = \eta_M/\eta_N(\rho_N g_N l_N^2/\rho_M g_M l_M^2)\nu_M$ (d)	1.4×10^{-6}	$4.78 \times 10^{-3 \text{ to } (-4)}$
	$6.7 \times 10^{-9 \text{ to } (-10)}$ ($\sim$0.2–2 cm y^{-1})		

(a) Weijermars et al. (1993); (b) Bonini (2001); (c) Cotton and Koyi (2000); (d) Weijermars and Schmeling (1986).

limestones; (c) an Early Cretaceous unconformity marked by hard ground on top of the Jurassic limestones; and (d) alternating pink pelagic marls and marly limestones, Late Cretaceous to Paleogene in age ('red beds'). In the western sector of the study area, the Subbetic rocks consist predominantly of Triassic evaporites, whose structural position and emplacement age are largely controversial. Flinch et al. (1996) proposed that these salt rocks were emplaced originally within Mesozoic sedimentary sequence in passive-margin setting. The diapiric allochthonous masses were then overthrusted as an accretionary wedge during the Miocene. By contrast, Bourgois (1978) claimed that the Triassic rocks are polygenetic breccias, formed during the Burdigalian, of Subbetic rocks in a gyspum cement.

The Aljibe thrust imbricate is the main tectonic unit of the Flysch Complex (Didon et al., 1973). The Paleogene sequence of this unit comprises claystones and intercalations of calcareous limestones, while the Neogene sequence is composed of a characteristic quartzite formation with minor marly levels, the Aljibe formation (Numidian of northern Africa; Didon et al., 1973). This formation has been dated as Aquitanian (Esteras et al., 1995). Structurally, the Aljibe thrust imbricate (Fig. 1) consists of an in-sequence leading imbricate fan (Boyer and Elliott, 1982) formed between the Late Burdigalian and the Langhian due to an approximately E–W shortening (Luján et al., 1999). This thrust wedge has been locally affected by a Serravallian extensional episode, and moderate-angle normal faults developed, as the fault which bounds the Aljibe and the Penibetic units, in the northeastern part of Fig. 1 (Luján et al., 2000).

No penetrative structures have been found in the field, and this indicates that rocks within the Aljibe thrust imbricate underwent a negligible amount of internal strain. In the eastern part of the study area (Fig. 1), tectonic windows show that the imbricated stack detached above Subbetic marly limestones (Late Cretaceous to Paleogene in age). In the western and northwestern parts, the same kind of exposures indicate that the sole thrust of the Aljibe thrust imbricate (Aljibe sole thrust) detached above Triassic evaporites. This variation of the substrate rocks below the Aljibe sole thrust closely coincides with a major change in structural style within the Aljibe thrust imbricate. In the eastern domain, thrusts and folds systematically verge towards the west, the width of the slices varying between 1 and 2 km, and their lateral continuity is frequently more than 20 km. On the other hand, the western domain is characterised by eastward-verging, irregularly spaced thrusts, moderate lateral continuity of map structures and extensive upright folding within the imbricate slices. The boundary between the two domains trends approximately N30°E and roughly coincides with the alignment of tectonic windows (Fig. 1). In the western domain, a second-order narrow transpressional zone running N50°E disrupts the continuity of the thrust imbricates (southwestern part of the map in Fig. 1).

3. Material properties and model kinematics

In the experiments, sand and silicone putty were used in a natural gravity field to simulate the rheological behaviour of sedimentary cover and salt rocks, respectively. Sand has long been recognized as an appropriate analogue material for simulating the Mohr–Coulomb behaviour of natural rock multilayers undergoing brittle deformation at shallow crustal levels (e.g. Davy and Cobbold, 1991). We used dry aolian quartz sand with a grain size varying between 0.2 and 0.3 mm, a coefficient of internal friction $\phi = 37.5°$, and density $\rho_b = 1.5$ g cm^{-3}, which exhibits a nearly perfect Mohr–Coulomb behaviour (shear tests in Acocella et al., 2000). Cohesion values are negligible up to 200 Pa under low normal stress conditions (triaxial and shear tests; E. Marotta, personal communication, 2002). Coloured sand was used to provide horizontal passive markers within the undeformed experimental multilayer. Silicone putty has been commonly used as Newtonian material with a strain-rate-dependent

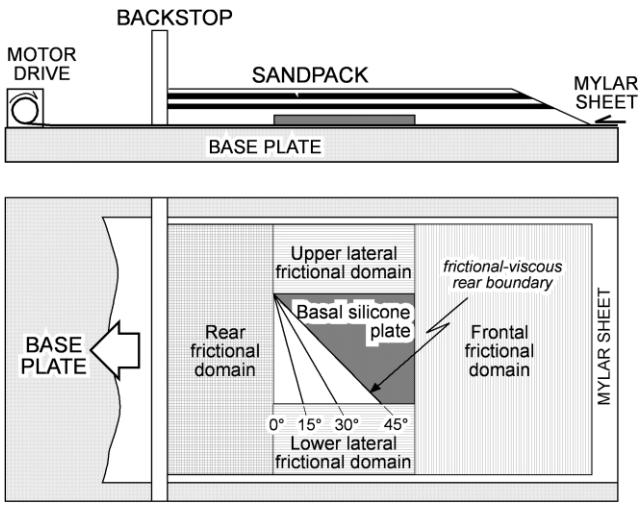

Fig. 2. Simplified sketch of the experimental apparatus and model setting in both cross-section and map view. The geometry of the basal silicone layer in different experiments (0, 15, 30 and 45° models) is schematically illustrated.

viscosity for modelling the ductile flow of incompetent décollement rocks like evaporites (e.g. Weijermars et al., 1993; Cotton and Koyi, 2000; Bonini, 2001). The silicone putty used in our experiments, manufactured by Rhodia (code 7007), had a density $\rho_v = 1.3\ g\ cm^{-3}$ and a viscosity $\eta = 1.2 \times 10^5$ Pa s at a constant shortening rate of 0.5 cm/h. For detailed rheology of this material and suitability as model analogue, see Weijermars (1986).

Table 1 shows the characteristic values of the four independent quantities—density (ρ), length (l), viscosity (η), and gravity (g)—for both natural prototype and analogue materials. The table also shows the corresponding scaling factors of the main physical parameters, according to the approach of Weijermars and Schmeling (1986). Scaling of the viscous décollement layer for an hour of model time t_M predicts a natural time t_N of about 0.04 to 0.4 Ma, and a natural velocity $v_N = 0.2$ to 2 cm y^{-1}, for the imposed model velocity $v_M = 1.4 \times 10^{-6}$ m s^{-1} (Table 1). These values are in good agreement with those of natural thrust systems and those obtained previously in similar analogue modelling experiments (e.g. Bonini, 2001).

The experiments were performed in a 100-cm-wide, 160-cm-long sandbox with no side walls, schematically illustrated in Fig. 2. A mylar sheet (coefficent of basal friction $\mu_b = 0.43$) floored the sandbox. A 0.5-cm-thick silicone plate with variable geometry was positioned above the mylar sheet in the central part of the experimental multilayers to simulate a basal evaporitic layer. An 80-cm-long, 50-cm-wide, 1.5-cm-thick sandpack was sieved above the mylar sheet and the central silicone plate, alternating coloured and uncoloured layers. A reference grid of 4-cm-sided squares was sieved onto the black top layer of the sandpack. The mylar sheet was pulled at a constant rate of 0.5 cm h^{-1} by an electric motor, causing collision of the undeformed multilayer against the rigid, vertical backstop provided by the end wall of the sandbox (Fig. 2). This forced collision induced the growth of a Coulomb wedge in the sandpack. The basal décollement of the sand wedge reached the silicone plate after about 20 cm of shortening. Total shortening was almost constant in all experiments, nearing 50% of the undeformed length of the sandpack. Different shapes of the silicone plate were used in different experiments. In particular, we varied the strike of the boundary of the silicone plate facing the backstop with respect to the strike of the backstop itself, which remained fixed. In the 0° model, the silicone had a rectangular shape, 27 cm long and 22 cm wide; in the 15, 30 and 45° models the angle between the strike of the silicone boundary and the backstop was 15, 30 and 45°, respectively (Fig. 2). The changing geometry was recorded by time lapse photography of the top surface. After completion, each model underwent serial sectioning parallel to the shortening direction. Duplication of the models allowed us to verify the reproducibility of the experimental results.

The experimental setup in our simple models does not account for plate flexure and isostatic compensation beneath the growing wedges, for the role of pore fluid pressure, and for the possibility of deformations affecting the backstop. These limitations are very common in sandbox experiments and have been shown not to significantly affect the first-order model results at the proper distance from the backstop (e.g. Malavieille, 1984; Liu et al., 1992; Koyi, 1995; Storti and McClay, 1995; Gutscher et al., 1996; Storti and Salvini, 2000; Bonini, 2001). We made relative comparisons among models constructed in the same experimental apparatus in order to prevent any significant influence of model limitations on our inferences.

4. Experimental results

In the early stages of shortening the whole wedge underwent noteworthy detachment along the mylar–sand boundary (rear frictional domain). With increased shortening, the basal décollement localised within the silicone layer in the central region of the multilayer (viscous domain) and remained located at the mylar–sand boundary in the lateral sectors (lateral frictional domains; Fig. 2).

4.1. Frictional domains

The progressive evolution of thrust wedge growth above the frictional domains was that of a typical Coulomb wedge in which the basal friction was slightly lower than the internal coefficient of friction of the wedge material (e.g. Mulugeta, 1988; Liu et al., 1992; Storti and McClay, 1995). Deformation was concentrated at the front of the wedge and the traces of the thrust faults were almost rectilinear. In the embryonic stage of wedge growth, i.e. when it was developing above the rear frictional domain, the strike of the backstop and the trace of the thrusts were parallel

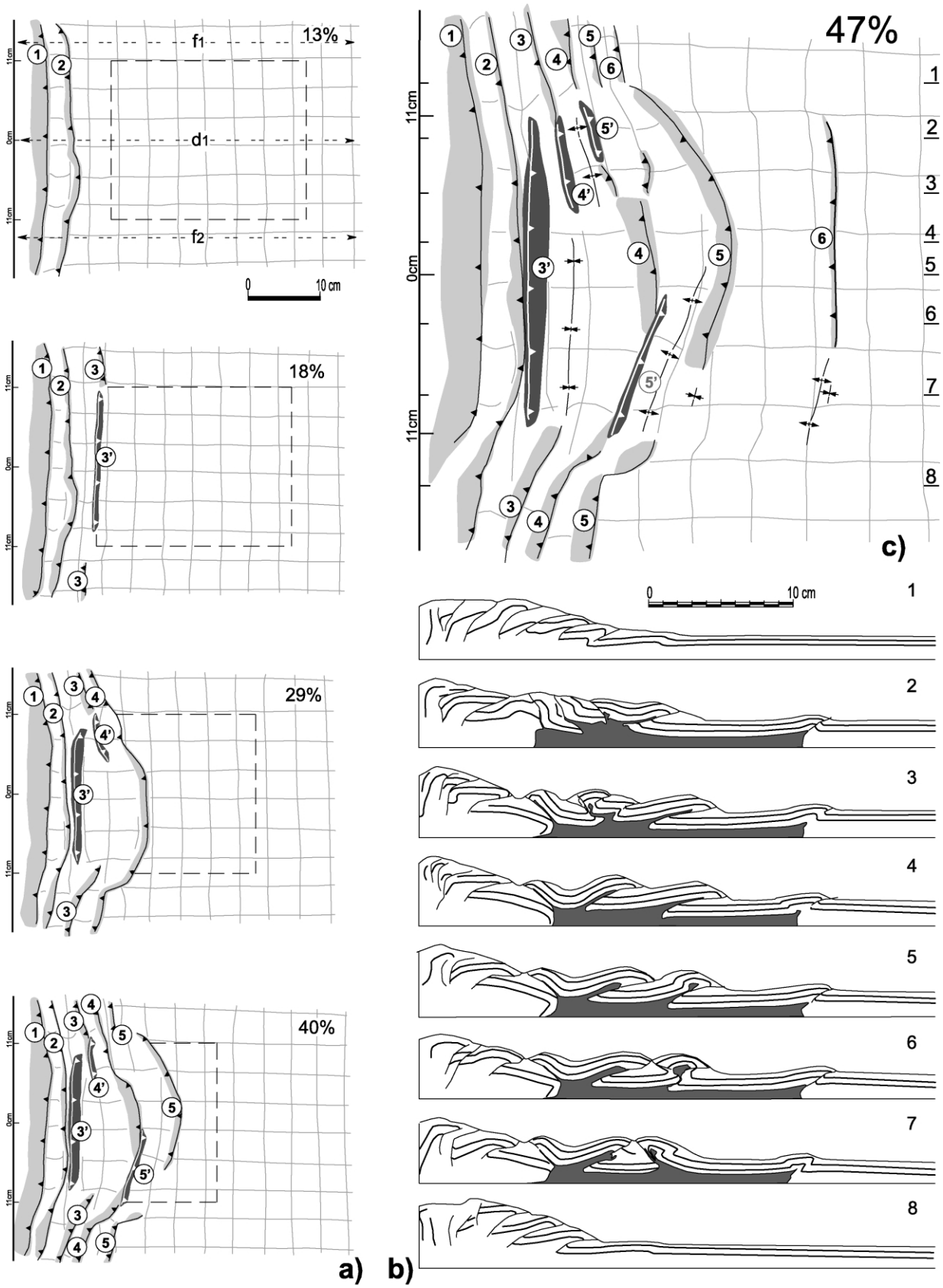

Fig. 3. Kinematic evolution and internal structure of the 0° model. (a) Line drawings of map view for various amounts of shortening indicated as percentage (redrawn from photos); light grey indicates slumped areas at the front of major thrusts, black indicates slumped areas at the front of major backthrusts; numbers indicate the nucleation sequence of the faults. (b) Serial cross-sections cut parallel to the tectonic transport direction at the end of the experiment. Locations are in (c). The silicone layer is highlighted by a dotted pattern. (c) Line drawing of the final stage of the 0° model and locations of serial cross-sections.

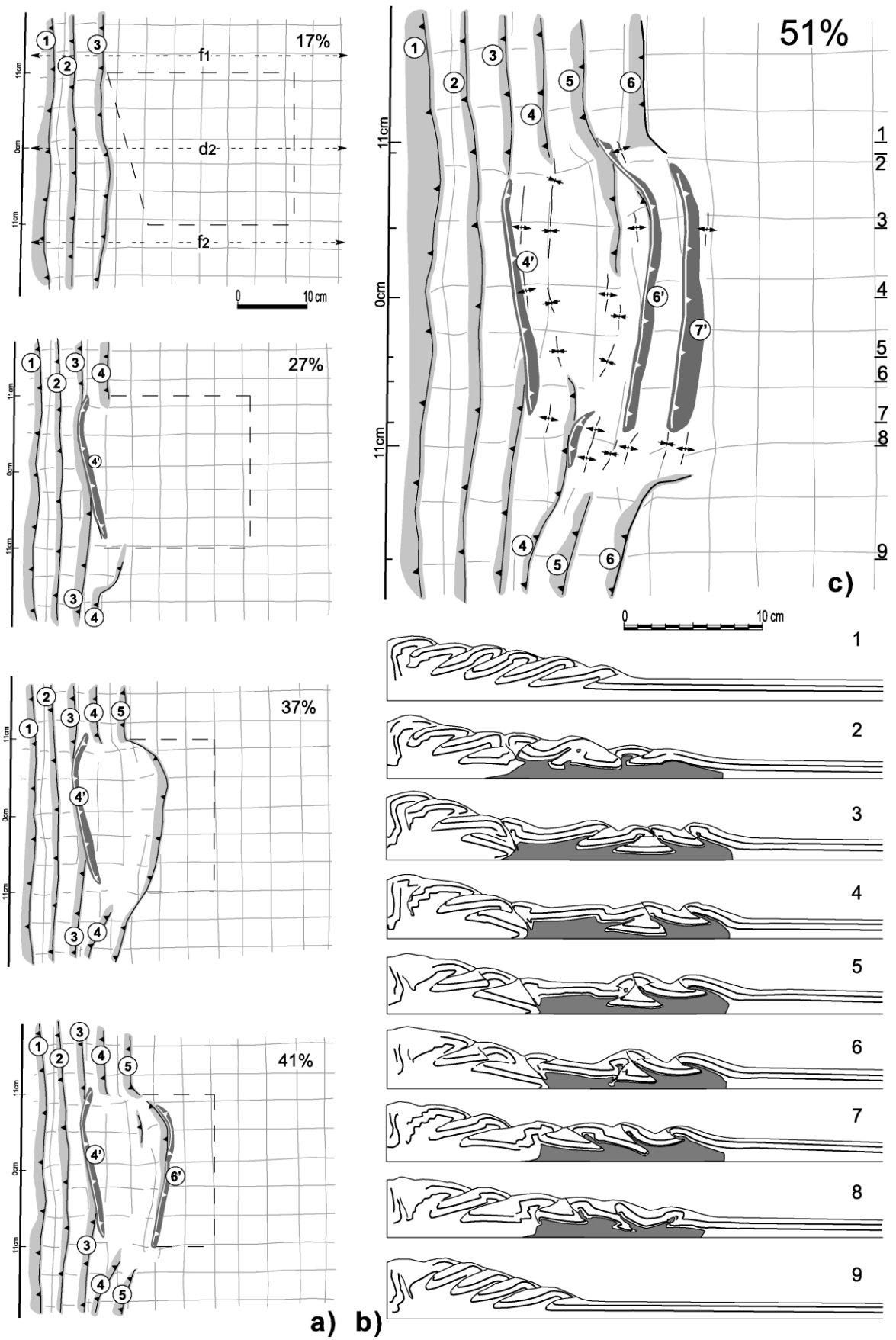
17%
f1
d2
f2
0
10 cm
27%
37%
41%
51%
11cm
0cm
11cm
0
10 cm
c)
a) b)

throughout the entire wedge (see the initial maps of thrusting sequence in Figs. 3a–6a). Mature Coulomb wedges developed in the lateral frictional domains, where they consisted of imbricates of foreland-verging thrusts. The imbricates were accreted in a piggyback fashion, producing wedges with surface tapers varying between 15 and 25°, depending on the amount of underthrusting of the frontal thrust sheet. The dip of the foreland-verging ramps progressively increased from the toe to the rear of the wedge, indicating passive backrotation of older thrust sheets during the accretion of new material at the toe (e.g. Liu et al., 1992; Mulugeta and Koyi, 1992). Backfolding and backthrusting were subordinate and mostly developed in the conjugate limbs of the box anticlines at the wedge toe during nucleation of new thrust sheets. Further development of these fault-related folds systematically led to thrust breakthrough and forelandward translation of the frontal anticlines (e.g. Storti and Salvini, 1997). The final geometry of thrust wedge sectors developed above the lateral frictional domains is illustrated in the first and last cross-sections of Figs. 3b–6b.

4.2. Viscous domain: general features

In all the experiments, where the sand wedge started propagating above the viscous substrate, a drastic change occurred in the deformation style. The forelandward structural asymmetry of the wedge ceased and a major backthrust generated, detached above the silicone. The subsequent thrust development showed no preferred vergence and included an approximately equal number of foreland- and hinterland-verging thrusts (Figs. 3–6). A new thrust wedge (external wedge) developed above the viscous substrate, juxtaposed against the older wedge (internal wedge) accreted above the rear frictional domain (Figs. 3b–6b). The surface taper of the external wedge decreased to much lower values, between 5 and 0°. This confirms the direct proportionality between surface wedge taper and basal friction (Davis and Engelder, 1985).

A striking difference involves the cross-sectional architecture of the two adjacent wedges (Fig. 7a): a simple foreland-verging leading imbricate fan characterises the internal wedge (e.g. Mulugeta, 1988; Liu et al., 1992; Koyi, 1995) whereas the external wedge shows a much more complex internal geometry of fault and fold arrays. The spacing between adjacent faults was much greater in the viscous domain than in the frictional domains. Overprinting and interference of former thrusts by younger backthrusts occurred in the viscous domain of the models (see 4 and 5′ in Fig. 3c).

Wide and gentle synclinal sectors, bounded by opposite-verging thrusts, are separated by narrow zones of intense faulting and folding, globally defining pop-up and pop-down structures (e.g. Letouzey et al., 1995; Cotton and Koyi, 2000). Both foreland- and hinterland-verging anticlines with large interlimb angles formed above layer-parallel décollements within the silicone plate. Thrust ramps frequently cut across the limbs of tighter anticlines, which eventually underwent either forelandward or hinterlandward thrust breakthrough and translation. This suggests that anticlines at the heads of thrust sheets formed by the temporal transition from décollement folding, to fault-propagation folding, up to fault-bend folding (Dixon and Liu, 1992; Storti and Salvini, 1997).

The asymmetrical load, produced by the weight of the internal wedge on the first thrust sheet of the external wedge, detached above the viscous layer, caused the outward squeezing of silicone, as indicated by the systematic downward-facing attitude of layering contiguous to the silicone (Figs. 3b–6b). The outward flow of the internal portion of the silicone plate caused it to almost double in thickness in the more external areas. The vertical flow of the ductile layer was enhanced by the pop-up structures, where ductile material was squeezed within the core of the anticlines, in places producing diapir-like structures (Fig. 7b). On the other hand, pop-down structures progressively sank into the viscous basal plate, acting as partial barriers to the forward migration of the silicone, as observed in cross-section 5 of the 15° model (Fig. 4b) (e.g. Cotton and Koyi, 2000). It is worth noting that density contrast in nature is lower than that of the analogue material ($\rho_{b_N}/\rho_{v_N} = 1.04$ vs $\rho_{b_M}/\rho_{v_M} = 1.15$, respectively, see Table 1). Consequently, buoyancy-driven processes are enhanced in the models.

The occurrence of a basal layer of viscous material facilitated the outward propagation of the deformation front in the central region of the experiments with respect to the lateral frictional domains. This modified the trace of the deformation front, from a rectilinear shape in the early stages of shortening, because to an outwardly convex shape with increased shortening. Consequently, structures noticeably non-cylindrical, as indicated by the abrupt changes in adjacent cross-sections of Figs. 3b–6b. Foreland-verging domains alternate along the strike with hinterland verging and rather symmetrical domains. A well developed salient (e.g. Macedo and Marshak, 1999) characterised the final stage of all experiments (Figs. 3c–6c).

Systematic monitoring of the distance of the deformation front from the backstop (D; Fig. 8) shows a typical saw-tooth shape, indicating that the thrust wedge growth occurred by discrete and abrupt widening pulses, separated by longer narrowing periods (Storti and Salvini, 2000). In all

Fig. 4. Kinematic evolution and internal architecture of the 15° model. (a) Line drawings of map view at different amounts of shortening. (b) Serial cross-sections cut parallel to the tectonic transport direction at the end of the experiment. Locations are in (c). (c) Line drawing of the final stage of the 15° model and locations of serial cross-sections.

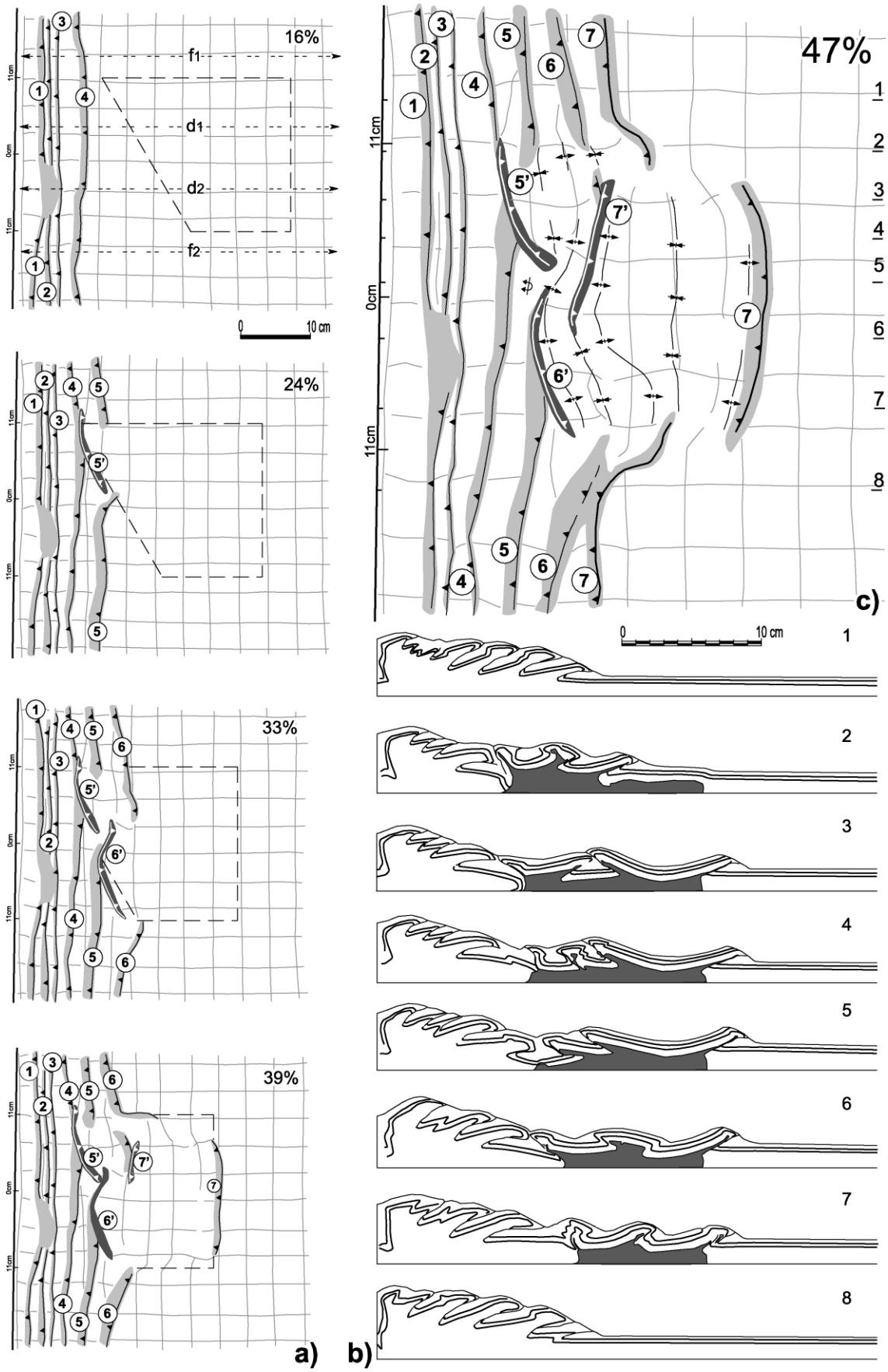
16%
f1
d1
d2
f2
0
10 cm
24%
33%
39%
a)
47%
11cm
0cm
11cm
c)
0
10 cm
1
2
3
4
5
6
7
8
b)

experimental configurations, the early evolutionary stages show very similar behaviours, in both the viscous and frictional domains (Fig. 8). In the viscous domain, the deformation rate along backthrusts was higher than along foreland thrusts, as shown by the increase in negative slope marked by segments that correspond to backthrusts (for example, segment 3′ of plot 0° model; Fig. 8). An abrupt increase of D values occurred in the viscous domain, whereas in the lateral regions of frictional substrate, D maintained its progression.

4.3. Viscous substrate: influence of geometry

The general features that are common to all experiments are complicated by specific geometric and kinematic patterns dictated by the shape of the viscous material. Differences are best expressed in map view. In the 0° model, the rear boundary between the frictional and viscous substrates was parallel to the backstop, i.e. perpendicular to the shortening direction (Fig. 2). When the wedge propagated above the basal viscous layer (18% of shortening), the first major backthrust formed parallel to the sand–silicone boundary. The younger major thrust (2 in Fig. 3a) and the newly-formed backthrust (3′) had the same strike. Two thrust segments formed in the lateral frictional domains (3), almost colinear to backthrust 3′. As a result of increasing shortening (29%) a wide frontal piggy-basin formed. The difference in deformation styles between viscous and frictional domains and the foreward jump of the deformation front across the basal silicone plate were accommodated by transfer zones striking parallel to the shortening direction (e.g. Cotton and Koyi, 2000). After 29% of shortening, the contractional structures showed an increasing curvature of their map traces as deformation progressed (Fig. 3a). This curvature was accommodated by thrusts and/or backthrust imbricates in the transfer zones parallel to the shortening direction, which was a feature common to all models.

In the 0° model, where the lateral viscous–frictional boundaries had the same length and were both parallel to the shortening direction, the final geometry was broadly symmetrical. Some of the passive markers situated within the transfer zone and originally parallel to the shortening direction showed rotations towards the lateral frictional domains, outwards to the arcuate thrust, like those located at the rear of thrust 5 (Fig. 3c). This implies that extension must have occurred along the trend of this particular thrust, as the length of the markers initially parallel to the backstop increased. Nevertheless, the small amount of extension, estimated at 6% by measuring the initial and final length of the markers, did not produce noticeable extensional structures.

In the 15° model, the rear boundary between the viscous and the frictional domains formed an angle of 15° to the backstop (Fig. 2). When the imbricate thrust fan began to propagate over the silicone substrate (27% of shortening), a backthrust formed parallel to the sand–silicone boundary, decapitating the pre-existing thrust-related anticline. An oblique accommodation zone was produced (Fig. 4a). The shape of the new frontal thrust was strongly influenced by the variable rheology at the bottom of the multilayer and a strongly arcuate thrust formed above the viscous domain (37% of shortening). An abrupt forelandward jump of the deformation front produced a wide piggyback basin in which out-of-sequence shortening occurred (Fig. 4a and c). The leading anticline bounding the piggyback basin forelandward was then decapitated by a newly-formed backthrust localised above the viscous domain (41% of shortening). In this model, more backthrusts than thrusts were produced above the viscous domain. Their strike was slightly oblique to the backstop and the resulting geometry was slightly asymmetric.

The 30° model was characterised by an angle of 30° between the frictional–viscous rear boundary and the backstop (Fig. 2), which resulted in strongly asymmetric 3D-structures. When the deformation front approached the viscous material (24% of shortening), a major backthrust formed near the upper corner of the silicone layer, parallel to the frictional–viscous rear boundary, and an oblique accommodation zone formed (Fig. 5a). At the same time, deformation in the central and lower sectors continued above a frictional décollement and a major thrust originated, striking parallel to the backstop. With increasing shortening, the deformation front was strongly segmented (33% of shortening). A major foreland-verging thrust segment propagated from the rear frictional domain into the upper half of the viscous domain, striking parallel to the backstop. Close to its termination, displacement was transferred to an outward-concave backthrust arranged in ‘en échelon’ fashion with the thrust. The major segment of the backthrust was almost parallel to the viscous–frictional boundary (Fig. 5a). A major outward jump of the deformation front occurred in the viscous domain at about 39% of shortening, while thrust spacing in the lateral frictional domains remained almost constant. A wide piggyback basin formed above the viscous domain and underwent out-of-sequence thrusting and folding with increased shortening (Figs. 5a and c and 9).

In the 45° model, the total volume of the silicone basal plate was reduced approximately to half that of the 0° model and the rear boundary between the frictional

Fig. 5. Kinematic evolution and internal structure of the 30° model. (a) Line drawings of map view at different amounts of shortening (redrawn from photos). (b) Serial cross-sections cut parallel to the tectonic transport direction at the end of the experiment. Locations are in (c). (c) Line drawing of the final stage of the 30° model and locations of serial cross-sections.

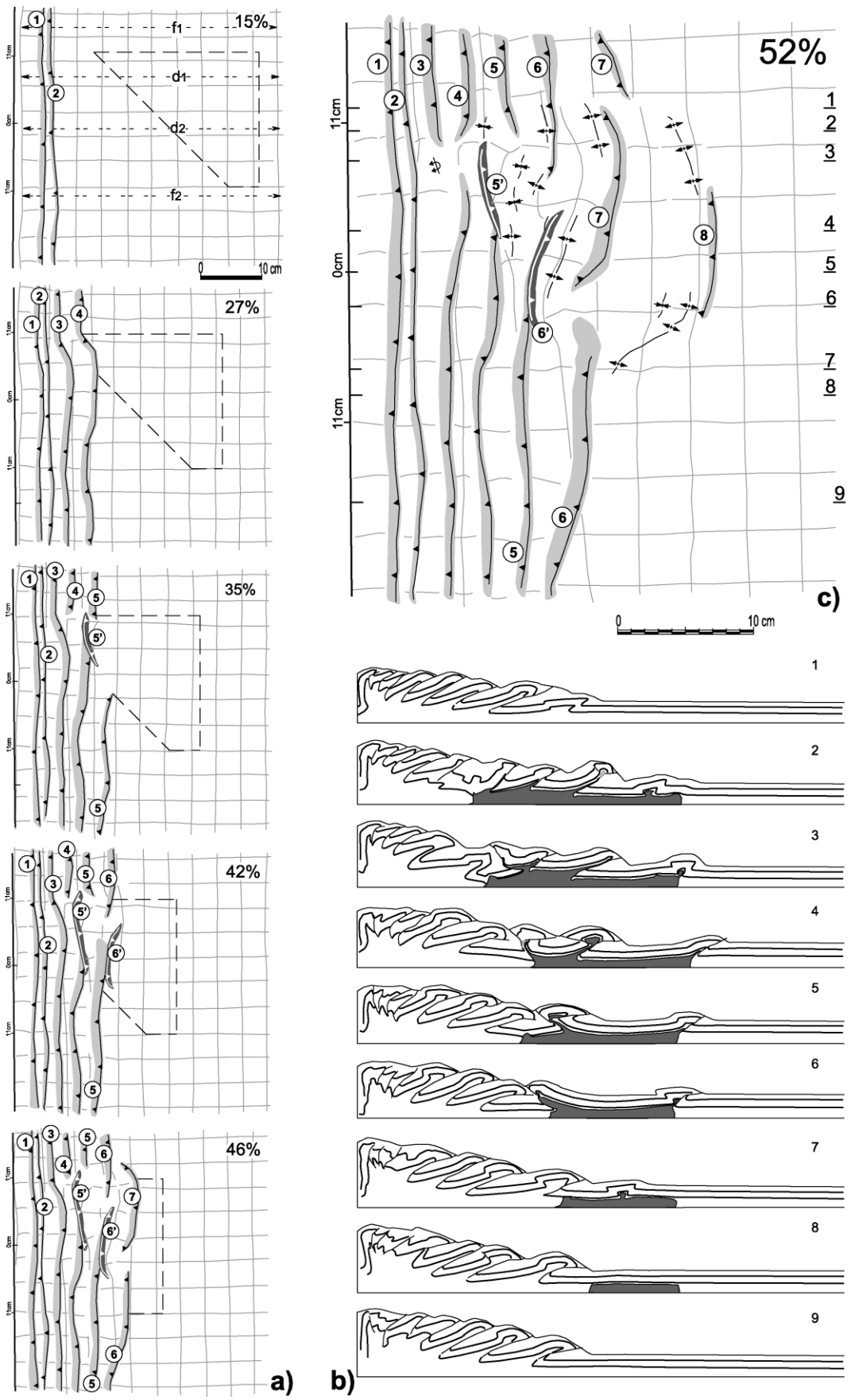
15%
f1
d1
d2
f2
0 10 cm
27%
35%
42%
46%
a)
52%
11cm
0cm
11cm
0 10 cm
c)
1
2
3
4
5
6
7
8
9
b)

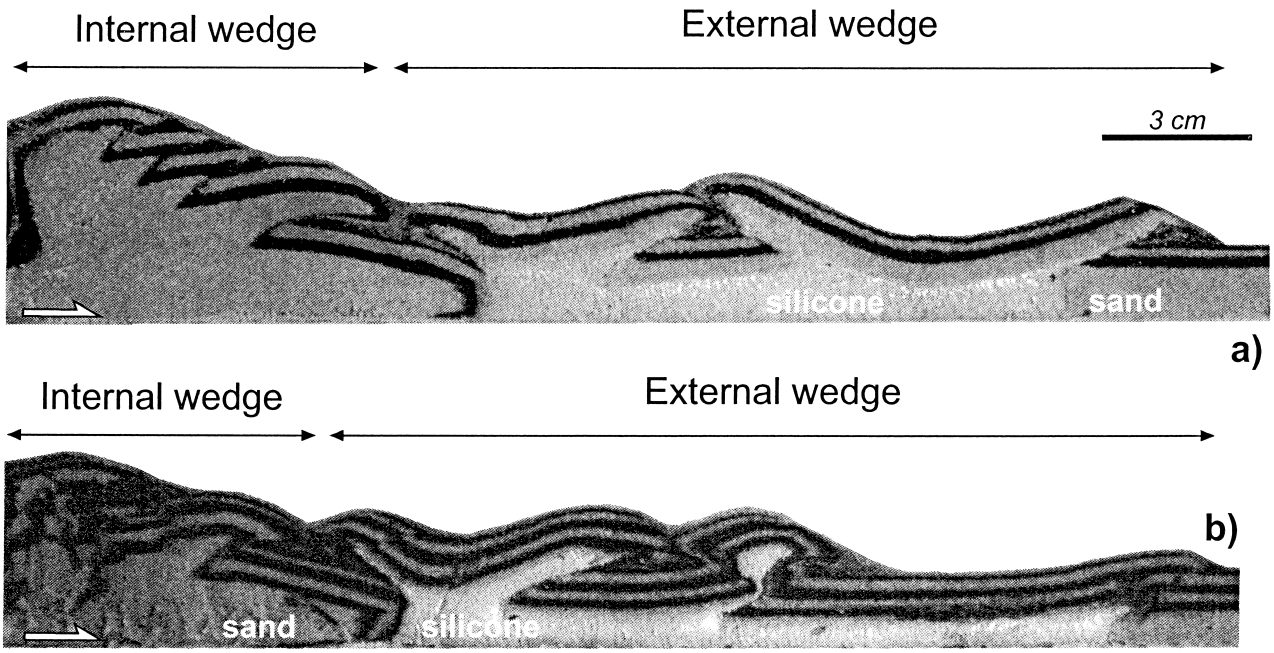

Fig. 7. Photographs representative of final cross-sections of the experimental wedges. (a) Section 3 of the 30° model (see Fig. 5), showing the striking difference of style occurring between the internal and external wedges above frictional and viscous substrate, respectively. (b) Section 6 of the 0° model (see Fig. 3), showing silicone putty squeezed in the core of an anticline of the external wedge.

and viscous domains formed an angle of 45° to the backstop (Fig. 2). The tendency to thrust segmentation highlighted in the 30° model was enhanced in this experiment due to the strong lateral variations of the area floored with viscous material. Consequently, the resulting geometry is the most asymmetric of all the models presented. The structural architecture of 45° model was governed by thrusts striking almost parallel to the backstop even when they propagated into the viscous domain. At 27% shortening, when the thrust wedge reached the sharp corner of the viscous domain, a small inflection of the frontal foreland thrust occurred. With increasing shortening, two short backthrusts originated in the viscous domain, interfering with a major thrust. Their overall strike was sub-parallel to the backstop (Fig. 6a). Only close to the end of the experiment did the deformation front reach the outer boundary of the silicone plate, producing a piggyback basin (52% of shortening). The envelope of the backthrust terminations, including second-order structures accommodating displacement transfer between thrusts and backthrusts, bounds a complex deformation zone, which strikes almost parallel to the frictional-viscous rear boundary (Fig. 6b and c).

To summarise, an increase of the angle between the frictional–viscous rear boundary and the backstop causes the following major effects: (1) a major asymmetry of the resulting 3D structure; (2) the length of the first-order backthrusts decreases; (3) the degree of fault segmentation increases; (4) the geometric correlation between the strike of the frictional–viscous rear boundary and that of the overlying faults decreases; and (5) the amount of shortening required for a development of the frontal piggyback basin increases.

5. Implications for the 3D structure of the Aljibe thrust imbricate

Striking features of the models described in this paper, which can be compared with structural features described in the Aljibe Unit, are: (1) the different style of deformation recognized between areas of the experimental wedge accreted above frictional (sand) or viscous (silicone) substrate; and (2) the final geometry of the shortened models, which can be directly correlated with the initial geometry of the viscous domain, as the asymmetric shapes of the viscous domain create accommodation zones oblique to the shortening direction.

Experimental wedge sectors that resulted from shortening above frictional domains are characterised by foreland-vergent thrusts and fault-related folds striking subperpendicular to the shortening direction (e.g. Liu et al., 1992). Thrust sheets are regularly spaced and continuous

Fig. 6. Kinematic evolution and internal structure of the 45° model. (a) Line drawings of map view at different amounts of shortening (redrawn from photos). (b) Serial cross-sections cut parallel to the tectonic transport direction at the end of the experiment. Locations are in (c). (c) Line drawing of the final stage of the 45° model and locations of serial cross-sections.

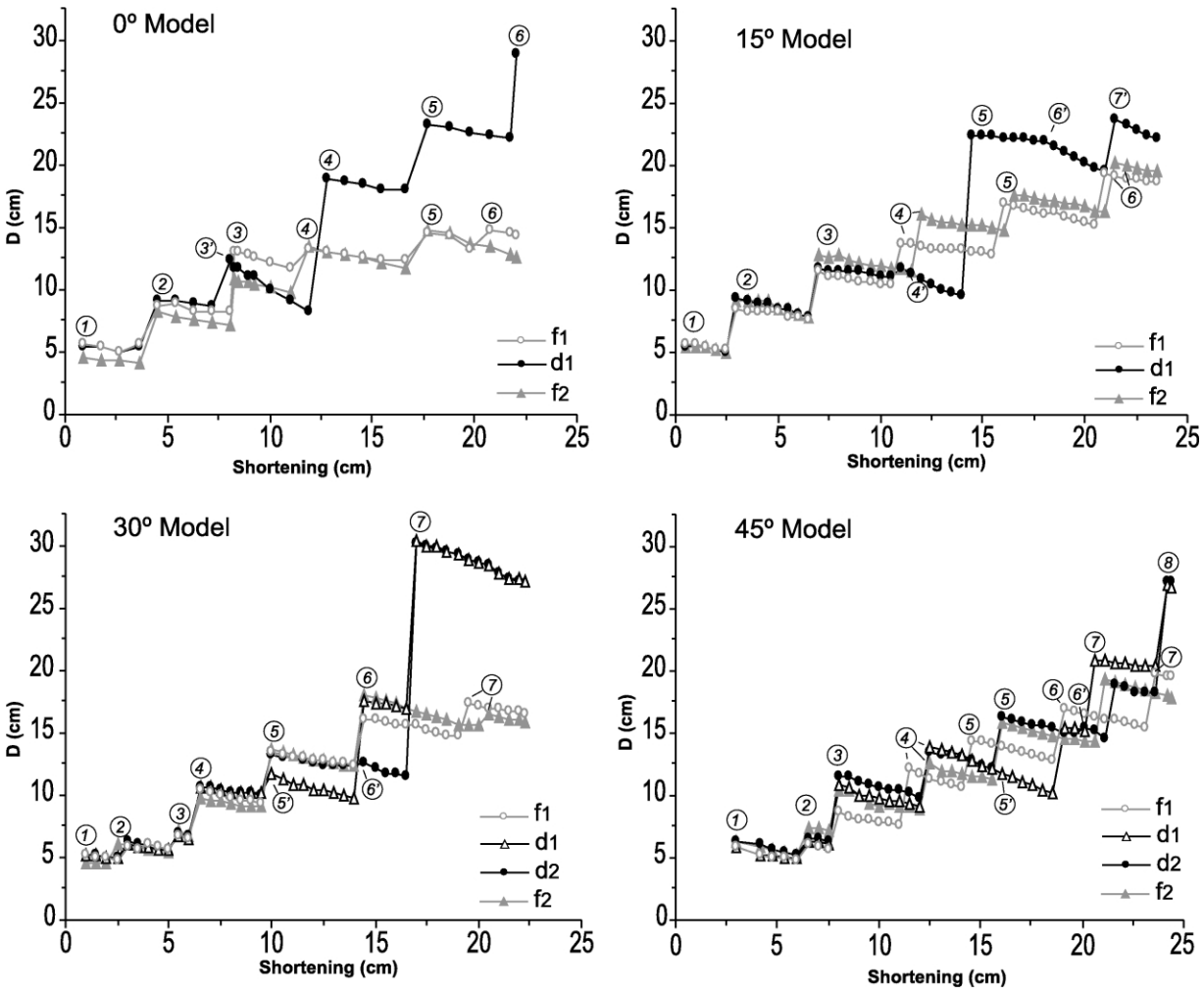

Fig. 8. Distance of the deformation front from the backstop (D) plotted against shortening. The numbers refer to numbered thrusts in the corresponding line drawings of map view in Figs. 3a–6a; f1 means that measurements were made along cross-sections including the upper lateral frictional domain (see Fig. 2); f2 means that measurements were made along cross-sections including the lower lateral frictional domain; d1 means that measurements were made along cross-sections including the upper half of the viscous domain; d2 means that measurements were made along cross-sections including the lower half of the viscous domain.

along strike. This structural style corresponds with that of the domain located east of the alignment of tectonic windows in the central part of the Aljibe thrust imbricate (Fig. 1). It contrasts with the deformation style described in the western domain of the study area, which shows hinterland- and foreland-vergent thrusts bounding irregularly-spaced thrust sheets with variable lengths. These thrusts are commonly arranged in pop-up and pop-down structures, and limit wide synclines with low amplitude/wavelength ratios. Such a structural style is characteristic of our models when shortening occurred above the viscous domain (Figs. 3–6). The comparison between the cross-section in Fig. 1 and the line drawing of section 5 in the 30° model highlights the similarity of the first-order structural architecture in nature and in the model (Fig. 10b).

From our laboratory data we infer that a change in rheological behaviour in the Subbetic substrate played a fundamental role in determining the contrasting structural styles developed in the western and eastern domains of the Aljibe thrust imbricate, respectively. The Subbetic substrate below the Aljibe thrust imbricate in the eastern domain corresponds to the highest frictional domains in the analogue models and must be made up essentially of competent limestones or marly limestones, which crop out in the easternmost tectonic windows. On the other hand, in the western domain the substrate of the Aljibe thrust imbricate would be provided by the Triassic evaporites, which outcrop in the westernmost tectonic window. The boundary between frictional and viscous substrate is inferred to be located in the central part of the Aljibe thrust imbricate, immediately west of the alignment of tectonic windows. Its approximate position is illustrated in Fig. 10a. The change of décollement material should have produced the main N30°E-trending accommodation zone, which is coherent with all the analogue models, where the first (and most internal) backthrust formed when the sand wedge began to propagate over the silicone plate.

The obliquity between the shortening direction and the

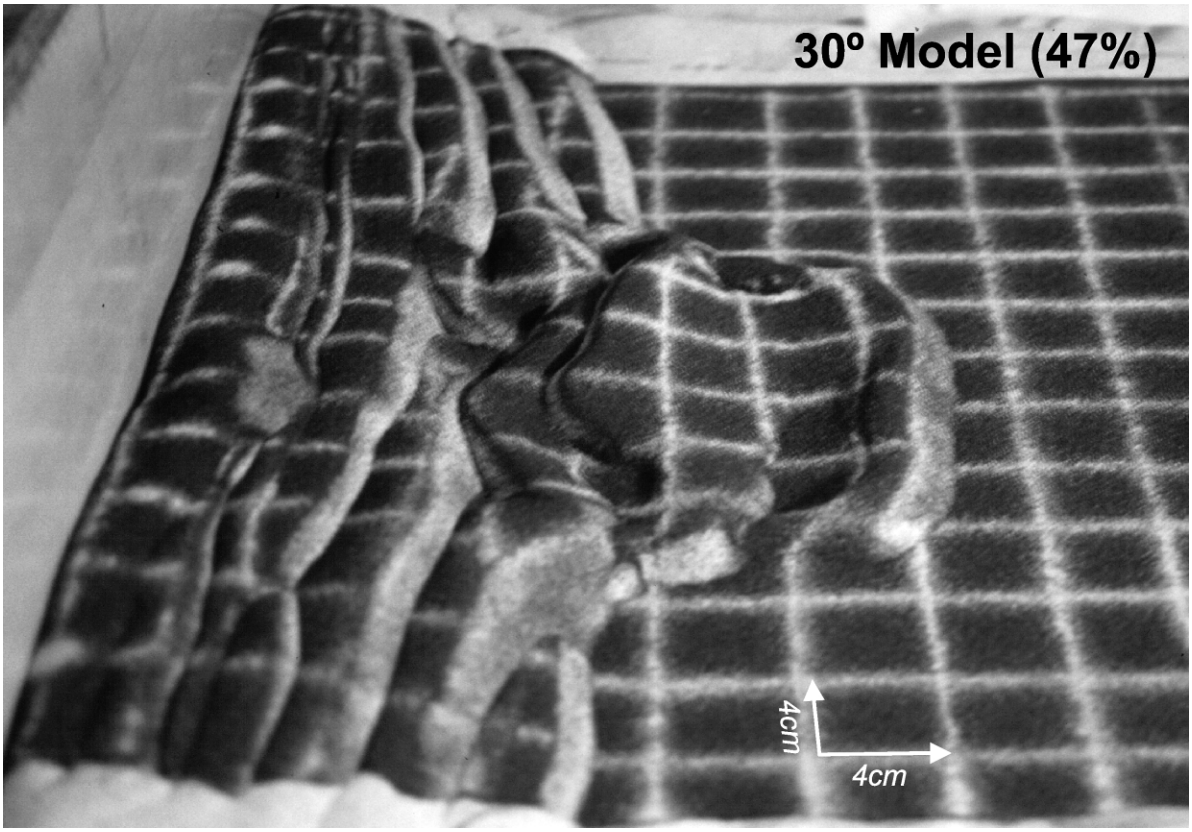

Fig. 9. Photograph showing an oblique view of the final stage of the 30° model.

frontal accommodation zone modelled in the asymmetric models (15, 30 and 45° models) suggests that in the natural example, the boundary between the frictional and ductile substrate is oblique with respect to the shortening direction. Kinematic indicators show a foreland transport direction in the Aljibe thrust imbricate towards the WNW (Fig. 1). This direction is at a high angle (about 75°) to the main N30°E-trending accommodation zone. Moreover, the striking similarity between 30° model and the natural example, both in map view and in cross-section (Fig. 10), suggests that the boundary between the limestones and the Triassic evaporites initially formed an angle of approximately 30° to the shortening direction.

In the previous sections, it has been shown that the western domain of the Aljibe thrust imbricate is divided into two parts by a transpressive zone, which runs approximately NE–SW (labelled S.T.Z. in Fig. 10). The origin of this second-order feature might be included in the variability range of structural trends developed above the viscous domain in asymmetric models. An alternative possibility to explain this N50°E-trending transpressional zone is to relate it to a change in the viscosity of the décollement material, due to a lithological variation. Indeed, the southernmost tectonic windows of Subbetic material show that upper Cretaceous to Paleogene rocks (red beds) form the substrate of the Aljibe thrust imbricate. The red beds are locally very rich in clay materials, which may have enhanced their viscous behaviour (Weijermars et al., 1993). Accordingly, it is suggested that this second-order accommodation zone within the viscous domain may be related to variations of viscosity at the footwall of the Aljibe unit sole thrust. These rheological variations are due to a change in lithology from evaporites to red beds.

The inference that the basal décollement of the Aljibe thrust imbricate is located in the evaporitic rocks towards the west raises a basic geometric and kinematic problem because it apparently implies a deepening of the sole thrust towards the foreland (from Paleogene to the east, to Triassic rocks to the west). This apparent problem can be overcome by relaxing the assumption of an undeformed foreland before contraction took place in the area. According to Flinch et al. (1996), a first diapiric emplacement of Triassic evaporitic rocks occurred during the Mesozoic–Cenozoic passive margin evolution of the South Iberian Domain. This diapiric event may have imparted the proper lithological heterogeneity to the South Iberian Domain for explaining the 3D variations of rock types constituting the substrate of the Aljibe thrust imbricate during its tectonic emplacement in a contractional environment. Shortening was probably driven by a push-from-behind mechanism, due to the westward migration of the

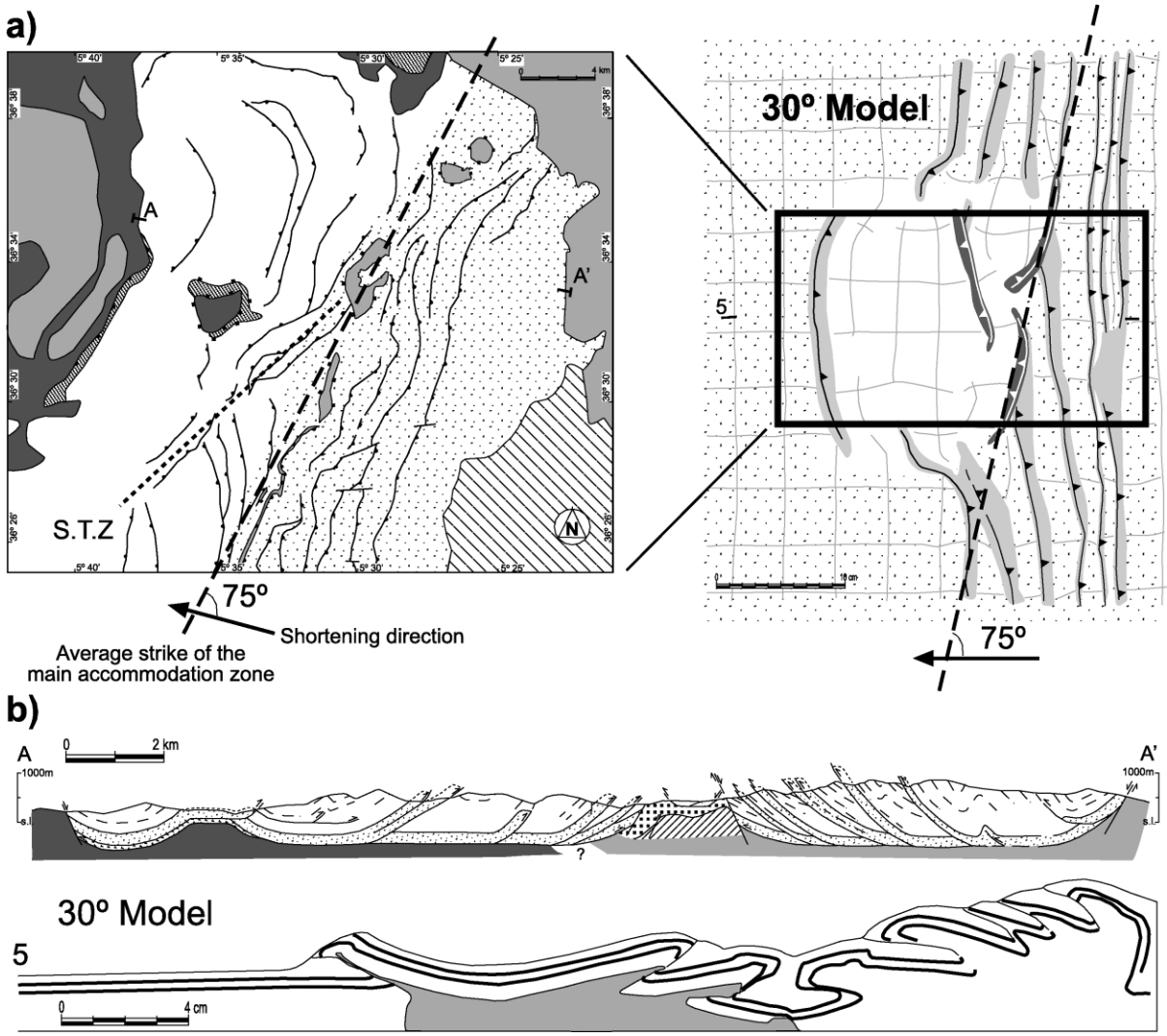

Fig. 10. (a) Comparison of natural example (to left) and analogue modelling (to right). The final stage of the 30° model has been reproduced as a mirror image to enhance the similarities. In both maps the frictional substrates have been underlined with dots. (b) Comparison of Aljibe unit cross-section and section 5 of the 30° model.

Alboran Domain—the internal zone of the Betics—which acted as the relatively rigid backstop of the accretionary wedge (Luján et al., 2000).

6. Conclusions

A set of analogue sandbox experiments was carried out to study the influence of 3D variations in rheological properties of décollement rocks on the structural architecture of a growing thrust wedge. Our results showed that the final geometry of the experimental thrust wedge is strongly influenced by the presence and geometry of a discontinuous viscous layer, modelled by silicone, at the base of the undeformed sandpack. Viscous material enhanced the development of major backthrusts and the outward migration of the deformation front.

Experimental results are closely comparable with the 3D structural architecture of the Aljibe thrust imbricate, situated in the external region of the Betic–Rif thrust wedge (Gibraltar Arc). The occurrence of two major structural domains and the trend and vergence of major thrust faults can be explained as a consequence of first-order variations in rock type along the basal décollement.

Acknowledgements

We are grateful to Claudio Faccenna for his suggestions and advice, and to P. Cobbold and W.P. Schellart for constructive reviews. This study was supported by grants from “Roma Tre” University (Italy) and by Grant PB96-0924 and BTE2000-0581 (Spain). We thank Jean Sanders for reviewing the English version.

References

Acocella, V., Faccenna, C., Funiciello, R., Rossetti, F., 2000. Sand-box modeling of basement-controlled transfer zones in extensional domains. Terra Nova 11/4, 149–156.

Balanyá, J.C., García-Dueñas, V., 1988. El cabalgamiento cortical de Gibraltar y la tectónica de Béticas y Rif. In: Sociedad Geológica de España. Actas, Segundo Congreso Geológico de España (Simposios), Granada, pp. 35–44.

Bonini, M., 2001. Passive roof thrusting and forelandward fold propagation in scaled brittle–ductile physical models of thrust wedges. Journal of Geophysical Research (B2) 106, 2291–2311.

Bonini, M., Sokoutis, D., Mulugeta, G., Katrivanos, E., 2000. Modeling hanging wall accommodation above rigid thrust ramps. Journal of Structural Geology 22/8, 1165–1179.

Bourgois, J. (Ed.), 1978. La transversale de Ronda (Cordillères Bétiques, Espagne). Données géologiques pour un modèle d'évolution de l'Arc de Gibraltar. Annales Scientifiques de l'Université de Besançon (France) 30.

Boyer, S., Elliott, D., 1982. Thrust systems. The American Association of Petroleum Geologists Bulletin 66/9, 1196–1230.

Burbank, D.W., Verges, J., Muñoz, J.A., Bentham, P., 1992. coeval hindward-imbricating and forward-imbricating thrusting in the South-Central Pyrenees, Spain—timing and rates of shortening and deposition. Geological Society of America Bulletin 104/1, 3–17.

Butler, R.W.H., Coward, H.P., Harwood, G.M., Knipe, R., 1987. Salt. Its control on thrust geometry, structural style and gravitational collapse along the Himalaya mountain front in the Salt Range of northern Pakistan. In: O'Brien, J.-J., Lerche, I. (Eds.), Dynamical Geology of Salt and Related Structures, Academic Press, London, pp. 399–418.

Cobbold, P.R., Rossello, E., Vendeville, B., 1989. Some experiments on interacting sedimentation and deformation above salt horizons. Bulletin de la Société Géologique de France 8/3, 453–460.

Cobbold, P.R., Szatmari, P., Demercian, L.S., Coelho, D., Rossello, E.A., 1995. Seismic and experimental evidence for thin-skinned horizontal shortening by convergent radial gliding on evaporates, deep-water Santos Basin, Brazil. In: Jackson, M.P.A., Roberts, D.G., Snelson, S. (Eds.), Salt Tectonics: A Global Perspective. American Association of Petroleum Geologists, Memoir 65, pp. 305–321.

Colman-Saad, S.P., 1978. Fold development in Zagros simply folded belt, southwest Iran. American Association of Petroleum Geologists Bulletin 62, 984–1003.

Cotton, J., Koyi, H., 2000. Modeling of thrust front above ductile and frictional detachments: application to structures in the Salt Range and Potwar Plateau, Pakistan. Geological Society of America Bulletin 112/3, 351–363.

Crespo-Blanc, A., Campos, J., 2001. Structure and kinematics of the South Iberian paleomargin and its relationship with the Flysch Trough units: extensional tectonics within the Gibraltar Arc fold-and-thrust belt (western Betics). Journal of Structural Geology 23/10, 1615–1630.

Davis, D.M., Engelder, T., 1985. The role of salt in fold-and-thrust belts. Tectonophysics 119, 67–88.

Davy, P., Cobbold, P.R., 1991. Experiments on shortening of a 4-layer model of the continental lithosphere. Tectonophysics 188, 1–25.

Didon, J., Durand-Delga, M., Kornporbst, J., 1973. Homologies géologiques entre les deux rives du Détroit de Gibraltar. Bulletin de la Société géologique de France 7/15, 77–105.

Dixon, J.M., Liu, S., 1992. Centrifuge modelling of the propagation of thrust faults. In: McClay, K.R., (Ed.), Thrust Tectonics, Chapman and Hall, London, pp. 53–69.

Durand-Delga, M., Rossi, P., Olivier, P., Puglisi, D., 2000. Situation structurale et nature ophiolitique de roches basiques jurassiques associées aux flyschs maghrébins du Rif (Maroc) et de Sicile (Italie). Comptes-Rendus de l'Académie des Sciences de Paris, Earth and Planetary Sciences 331, 29–38.

Esteras, M., Feinberg, H., Durand-Delga, M., 1995. Nouveaux éléments sur l'âge des grès numidiensde la nappe de l'Aljibe (Sud-Ouest de l'Andalousie, Espagne). Abstracts of Proceedings, IV Coloquio Internacional sobre el enlace Fijo del Estrecho de Gibraltar, Sevilla, SECEG.

Flinch, J., Bally, A., Wu, S., 1996. Emplacement of a passive-margin evaporitic allochthon in the Betic Cordillera of Spain. Geology 14/1, 67–70.

Geiser, P.A., 1988. Mechanisms of thrust propagation: some examples and implications for the analysis of overthrust terranes. Journal of Structural Geology 10, 829–845.

Gutscher, M.A., Kukowski, N., Malavieille, J., Lallemand, S., 1996. Cyclical behavior of thrust wedges—insights from high basal friction sandbox experiments. Geology 24/2, 135–138.

Harrison, J.C., Bally, A.W., 1988. Cross-sections of the Parry Island foldbelt on Melville Island. Canadian Petroleum Geologist Bulletin 81, 398–423.

Koyi, H., 1995. Mode of internal deformation in sand wedges. Journal of Structural Geology 17/2, 293–300.

Laubscher, H.P., 1972. Some overall aspects of the Jura dynamics. American Journal of Science 272, 293–304.

Letouzey, J., Colletta, B., Vially, R., Chermette, J.C., 1995. Evolution of salt-related structures in compressional settings. In: Jackson, M.P.A., Roberts, D.G., Snelson, S. (Eds.), Salt Tectonics: A Global Perspective: American Association of Petroleum Geologists Memoir 65, pp. 41–60.

Liu, H., McClay, K.R., Powell, D., 1992. Physical models of thrust wedges. In: McClay, K.R., (Ed.), Thrust Tectonics, Chapman and Hall, London, pp. 71–81.

Luján, M., Crespo-Blanc, A., Balanyá, J.C., 1999. Structure and kinematics of the Aljibe Unit, north of Cádiz Province (Flysch Trough Complex, Betics). Geogaceta 26, 47–50.

Luján, M., Balanyá, J.C., Crespo-Blanc, A., 2000. Contractional and extensional tectonics in Flysch and Penibetic units (Gibraltar Arc, SW Spain): new constraints on emplacement mechanisms. Comptes-Rendus de l'Académie des Sciences de Paris, Earth and Planetary Sciences 330, 631–638.

Macedo, J., Marshak, S., 1999. Control on the geometry of fold–thrust belt salients. Geological Society of America Bulletin 111/12, 1808–1822.

Malavieille, J., 1984. Modélisation expérimentale des chevauchements imbriqués: Application aux chaînes de montagnes. Bulletin de la Société Géologique de France 26, 129–138.

Mulugeta, G., 1988. Modelling the geometry of Coulomb Thrust wedges. Journal of Structural Geology 10, 847–859.

Mulugeta, G., Koyi, H., 1992. Episodic accretion and strain partitioning in a model sand wedge. Tectonophysics 202, 319–333.

Ryan, W.B.F., Kastens, K.A., Cita, B.M., 1982. Geological evidence concerning compressional tectonics in the Eastern Mediterranean. Tectonophysics 86, 213–242.

Storti, F., McClay, K., 1995. Influence of syntectonic sedimentation on thrust wedges in analogue models. Geology 23, 999–1002.

Storti, F., Salvini, F., 1997. Fault-related folding in sandbox analogue models of thrust wedges. Journal of Structural Geology 19/3– 4, 583–602.

Storti, F., Salvini, F., 2000. Synchronous and velocity-partitioned thrusting and thrust polarity reversal in experimentally produced, doubly-vergent thrust wedges: implications for natural orogens. Tectonics 19/2, 378–396.

Talbot, C.J., 1992. Centrifuged models of Gulf of Mexico profiles. Marine and Petroleum Geology 2, 412–432.

Velaj, T., Davison, I., Serjani, A., Alsop, I., 1999. Thrust tectonics and the role of evaporites in the Ionian Zone of the Albanides. American Association of Petroleum Geologists Bulletin 83, 1408–1425.

Weijermars, R., 1986. Flow behavior and physical chemistry of bouncing putties and related polymers in view of tectonic laboratory applications. Tectonophysics 217, 143–174.

Weijermars, R., Schmeling, H., 1986. Scaling of Newtonian and non-Newtonian fluid dynamics without inertia for quantitative modelling of rock flow due to gravity (including the concept of rheological similarity). Physics of the Earth Planetary Interior 43, 316–330.

Weijermars, R., Jackson, M.P.A., Vendiville, B., 1993. Rheological and tectonic modeling of salt provinces. Tectonophysics 217, 143–174.